🔓 OPEN ACCESS

Human stem cells with in vivo high plasticity generated by cell–cell communication

Shaowei Li[a], Xi Chen[b,1], Jingxue Xin[b,1], Bowen Liu[a,1], Bo Liu[a], Min Hu[a,2,3], and Wing Hung Wong[b,c,d,2,3] (iD)

Affiliations are included on p. 10.

Stem cells possess inherent properties of self-renewal and differentiation, and thus hold significant promise for regenerating damaged tissues or replacing lost cells. Unless their therapeutic effects are solely mediated by paracrine, transplanted stem cells need to be highly plastic to adapt to the host tissue environment and differentiate into constituent tissue-specific cells for tissue repair. Stem cells used in current cell-based therapies either have limited differentiation potential or are pluripotent but must be strictly restricted to avoid tumorigenicity risk in vivo. Here, we describe the derivation of human adult high-plasticity stem cells, which we call guide-integrated adult stem cells (giaSCs), from the interaction of blood-derived guide cells and umbilical cord tissue–derived mesenchymal stromal cells (UC-MSCs). The guide cells are a cell population derived from the peripheral blood of human adults. Unidirectional transfer through nanotube-like structures of granular substances from the guide cells into the recipient UC-MSCs gave rise to giaSCs. Topical application of human giaSCs into full-layer excisional wounds of wild-type mice led to reconstitution of skin tissue. Systemically administered human giaSCs migrated to and reside in mouse small intestinal tissue damaged by lipopolysaccharides and then differentiated into small intestinal epithelial cells for tissue repair. These transplantation experiments demonstrated that giaSCs have in vivo high plasticity. Additional in vivo and in vitro data showed that giaSCs have low immunogenicity and are nontumorigenic. These data indicate that giaSCs offer a highly promising approach to stem cell therapy.

stem cell | tissue repair | plasticity | intercellular communication | transcriptomic analysis

Stem cells, based on their inherent properties of self-renewal and multidirectional differentiation, renew or replace aging and apoptotic cells under physiological conditions to maintain tissue homeostasis (1, 2). Under pathological conditions, stem cells may also be able to integrate into the relevant pathological tissue leading to structural and functional restoration in the tissue (2, 3). Stem cell therapies are now used to treat a number of diseases. As a paradigm, hematopoietic stem cells (HSCs), which are restricted to blood and immune cell lineage differentiation, are used in treatment of a variety of refractory blood diseases, such as leukemia (3). After myeloablative treatment, transplanted HSCs self-renew and differentiate into all types of blood cells to reconstitute the entire blood tissue (3, 4).

Tissues in the body are in highly organized structures composed of a multitude of cell types that originate from different germ layers. For example, the multitype constituent cells in skin tissue are derived from ectoderm and mesoderm (5, 6). Stem cells with the potential to differentiate across germ layers are necessary for maintenance of tissue homeostasis and repair or reconstitution of tissues at the systemic level. In humans, natural pluripotent stem cells (embryonic stem cells) are present transiently during early embryonic development (7). Induced pluripotent stem cells can be artificially generated in vitro from somatic cells through a reprogramming process (8). These pluripotent stem cells have the potential to differentiate into all cell types in the body (9, 10) and should, in theory, have the capability to repair damaged tissues and reconstitute tissues at the systemic level. However, in practice pluripotent stem cells cannot be directly transplanted into recipients due to the high probability of tumorigenesis (11, 12). To harness the pluripotent differentiation potential of pluripotent stem cells for therapy, differentiation must be strictly directed through artificially regulated differentiation (i.e., "de-stemness") into the desired, terminally differentiated cells in vitro before transplanting into recipient (13, 14). Without this de-stemness step, there is a risk of tumor formation after transplantation. However, upon differentiation into a single target cell type in vitro, the cells may lose the ability to reconstitute tissue composed of multiple cell types. As the cellular plasticity is reduced or entirely eliminated, terminally differentiated cells are less capable of adapting to the host

Significance

Stem cells with high plasticity possess the potential to repair damaged tissue by differentiating into constituent tissue-specific cell types. Stem cells used in current cell-based therapies either have limited differentiation potential or are pluripotent but must be strictly restricted to avoid tumor formation. This paper describes the characterization of a distinct stem cell, which we call guide-integrated adult stem cells (giaSCs), generated from the interaction between blood-derived guide cells and mesenchymal stromal cells derived from umbilical cord tissue. Human giaSCs have high plasticity and can repair skin wounds and small intestinal tissue damage in wild-type mouse models without causing acute immune rejection or tumors. Thus, these cells have potential for use in regenerative medicine.

[1]X.C., J.X., and Bowen Liu contributed equally to this work.

[2]M.H. and W.H.W. contributed equally to this work.

[3]To whom correspondence may be addressed. Email: minhu@apstemtx.com or whwong@stanford.edu.

tissue environment after transplantation in vivo, which can cause pathological effects. For example, cardiomyocytes differentiated from induced pluripotent stem cells often cannot coordinate with the host myocardial rhythm after transplantation into the host heart tissue leading to arrhythmia (15, 16).

The ideal stem cells for therapy should retain their high plasticity but not result in tumorigenesis. Preserving in vivo high plasticity allows the stem cells to adapt to the local tissue environment, reside in tissue sites requiring repair, and participate in tissue reconstitution. High plasticity stem cells may differentiate across germ layers into the constituent cells of local tissue, and may also exert paracrine (e.g., anti-inflammatory and angiogenic) effects to facilitate tissue reconstitution. In this study, we describe a type of stem cell that fulfills these criteria. This type of stem cell is generated via communication between two types of somatic cells: mature guide cells (m-GCs) derived from human peripheral blood and mesenchymal stromal cells derived from human umbilical cord tissue (UC-MSCs). The precursors to the m-GCs are nucleated cells, 2 to 6 μm in diameter and in a dormant state. After overnight culture in a special medium, more than 90% of GCs are activated, and after 2 to 3 wk in culture the cells develop into m-GCs. A distinctive sign of the maturation is accumulation of RNA-containing cytoplasmic granules. The m-GCs establish structural channels to the UC-MSCs that resemble tunneling nanotubes (TNTs) (17). Through these TNT-like channels, m-GCs unidirectionally transport the RNA-rich granules into UC-MSCs. Bioinformation from these granules is integrated in UC-MSCs, leading to changes in their gene expression profile and thus converting them into a type of stem cell that we call guide-integrated adult stem cells (giaSCs). By extensive transplantation experiments using wild-type mice, giaSCs were shown to have in vivo high plasticity and low immunogenicity, and no tumorigenicity when transplanted into immunodeficient mice. Given these desirable properties, giaSCs warrant further study.

Results

Properties That Make giaSCs Promising in Regenerative Medicine.

giaSCs have in vivo high plasticity. We tested the in vivo plasticity of human giaSCs in mouse models of skin wounds and small intestinal tissue damage. In the skin tissue reconstitution assay (18), human giaSCs were mixed with a human fibrin gel and were topically transplanted into full-thickness skin wounds in mice. The fibrin gel is biodegradable thus allowing slow release of cells as the gel degrades in the local tissue. It has been widely used as a cell carrier or scaffold in tissue engineering (19, 20) and is therefore employed here as a scaffold for human giaSCs in topical treatment. In a pilot study, we had used immunodeficient mice (nude) to evaluate the human giaSC/fibrin gel treatment, which resulted in smooth skin healing on day 20 with revascularization (*SI Appendix*, Fig. S1 *A and B*) compared to control nude mice treated with saline. Histological analysis showed skin structural reconstitution (*SI Appendix*, Fig. S1*C*), in which human Ku80+ cells derived from giaSCs at the wound sites post human giaSC/fibrin gel treatment were detected (*SI Appendix,* Fig. S1*D*). These results motivated us to further investigate the efficacy of human giaSC/fibrin gel in immunocompetent wild mice (FVB). The giaSC/fibrin gel treatment accelerated wound closure (i.e., reduction of wound area percentage, Fig. 1*A*) when compared to controls treated with UC-MSCs in fibrin gel, fibrin gel only, and saline respectively. Fig. 1*A* shows that the wounds treated with giaSCs closed faster starting on day 3 compared with the other three control groups. On day 15, there were significant

differences ($P < 0.05$) between wounds treated with giaSCs and all three control groups. giaSCs treatment resulted in complete wound healing on day 15, about 5 d (25%) faster than that of control groups.

Histological analysis demonstrated wounds treated with giaSC/fibrin gel achieved full-thickness regeneration, showing a flat and smooth epidermal tissue without shrinkage, much fewer collagen fibers, and abundant neofollicles (Fig. 1*B* and *SI Appendix*, Fig. S2*B*). In contrast, the quality of regenerated dermal tissue in all control groups was poor although the wounds closed on day 20 (*SI Appendix*, Fig. S2*A*). Their wound closures were mainly due to scar contraction evidenced by large amounts of collagen fibers forming scar tissues (Fig. 1*B* and *SI Appendix*, Fig. S2*B*). A specific anti-human Ku80 antibody is commonly used to identify human cells in mouse tissues (21). In mouse skin treated with giaSCs, human giaSC–derived cells (human Ku80+) were detected in ectoderm-originated tissues such as epidermal basal cells, sebaceous glands (Fig. 1*C*), and hair follicles (Fig. 1*D* and *SI Appendix*, Fig. S2*C*) as well as in mesoderm-originated tissues such as blood vessels, muscle tissue (Fig. 1*E*), and adipose tissue (*SI Appendix*, Fig. S2*D*). Both human Ku80+ cells derived from giaSCs and human Ku80- cells (i.e., mouse endogenous cells) were present in the reconstituted tissue. To further confirm the presence of human giaSC–derived cells with orthogonal evidence, we performed in situ hybridization using a biotinylated DNA probe targeting human Alu gene fragment, which are primate-specific repeats and have been widely used for discriminating human cells from rodent cells. Positive Alu signals were observed in mouse wound tissue (especially the hair follicles) treated with human giaSC/fibrin gel (*SI Appendix*, Fig. S3*A*), which is consistent with the Ku80 IHC staining results. These results indicate that on day 20, when the skin wounds were repaired, cells of human origin (i.e., derived from human giaSCs) resided in local constituent tissue.

In addition, human giaSCs expressed anti-inflammatory factor CD73 as shown by flow cytometry (*SI Appendix*, Fig. S4) and by RNA sequencing (*SI Appendix*, Fig. S5*A*) and the mRNA encoding immune modulator TGF-β1 (*SI Appendix*, Fig. S5*B*). These factors expressed by giaSCs led us to speculate that they may have immune modulatory effects in vivo, which will be investigated in future studies. Human giaSCs also express the transcripts encoding growth factor VEGF (*SI Appendix*, Fig. S5*C*), indicating their potential to promote angiogenesis. Consistently, image analysis of the medial surface of the skin showed that significantly larger area of vascular networks were present in the wound sites on day 20 after giaSC/fibrin treatment compared to the control groups (Fig. 1*F*).

We used lipopolysaccharides (LPS) to induce small intestine damage of wild-type (FVB) mice to test the ability of the transplanted cells to migrate to and reside in damaged tissue and to facilitate tissue repair through systematic cell administration. LPS causes extensive small intestinal injury including damage to intestinal integrity and destruction and shortening of the villi (22). Human giaSCs labeled using Qtracker 625, a red fluorescent dye, were transplanted via retro-orbital injection into mice treated with LPS. Control mice received Qtracker 625 labeled human UC-MSCs or just saline. Eight of 10 (80%) giaSC-treated mice survived (on day 8); while five of 10 mice (50%) treated with UC-MSCs and four of eight (50%) treated with saline survived. On day 8 after treatment, the small intestine ileums were collected from each mouse, and histological evaluation was performed. Villus heights were significantly greater in the mice treated with giaSCs than in that of control mice (Fig. 1*G*), indicating higher efficacy in LPS-induced intestinal injuries treated by giaSCs compared to that in control groups. Red fluorescent signals from giaSCs-derived cells

were detected in the crypts, at the bottom of the mucosal layer, and along the villi of the treated mice (Fig. 1H). The fluorescent signals coincided with locations of human Ku80⁺ cells detected by IHC (Fig. 1 *I–K*). Many human Ku80⁺ giaSC-derived cells exhibited simple columnar epithelial morphology, originating from the crypts up both sides of the villi (Fig. 1 *I* and *J*), indicating that human giaSCs had differentiated into enterocytes that had repopulated the mouse's damaged area. The upper parts of the villi were mainly composed of mouse simple columnar epithelial cells, with sporadic human Ku80⁺ cells (Fig. 1*I*). Human giaSC–derived cells were also observed in the smooth muscle layer of the small intestine and in the adipose tissue cells on the mesentery (Fig. 1*K*). As orthogonal evidence to the Ku80 IHC data, we also generated Alu ISH data. In situ hybridization using the biotinylated Alu probe showed the presence of Alu⁺ cells (human giaSC–derived cells) aligning the villi (showing simple columnar epithelial morphology) as well as in the crypts (*SI Appendix*, Fig. S3*B*), which was consistent with the distribution pattern of the human Ku80⁺ cells (IHC staining). Double immunofluorescence staining using antibodies specific for human and mouse ki67 antigens, respectively, revealed the presence of proliferating human cells derived from giaSCs and endogenous mouse cells in the small intestine villi of the mice treated with human giaSCs (*SI Appendix*, Fig. S3*C*). The morphology of the giaSC-treated small intestines resembled that of normal small intestinal epithelium (Fig. 1 *I* and *M*).

No red fluorescent signal was detected in the small intestinal tissues in the LPS-damaged mice treated with Qtracker 625 labeled human UC-MSCs, (Fig. 1*H*), and no human Ku80⁺ cells were detected either (Fig. 1*L*). Villus shortening and structural damages were evident (Fig. 1 *G* and *L*). In saline-treated LPS mice, small intestinal tissues were damaged but no human Ku80⁺ cells were detected (*SI Appendix*, Fig. S2*E*). No human Ku80⁺ cells were detected in the healthy small intestinal tissues of wild-type (FVB) mice without LPS damage, after retro-orbital injection of giaSCs (Fig. 1*M*). This indicated that human giaSCs do not reside in small intestinal tissues under normal physiological conditions but only present, migrate, and reside in the damaged small intestine, and differentiated into small intestinal epithelial cells to participate in the repairing process.

giaSCs have low immunogenicity. The experiments described above demonstrate that human giaSCs were able to survive and integrate into immunocompetent wild-type mice for a duration sufficient to significantly promote tissue repair, suggesting that they do not elicit an acute immune response that might prevent their participation in the tissue repair. Transcriptomics analysis (RNA-seq) shows low immunogenicity of human giaSCs with very low expression of mRNAs encoding HLA-I proteins (i.e., HLA-A, -B, and -C), and undetectable expression of mRNAs encoding HLA-II proteins (i.e., HLA-DR, -DP, and -DQ) (*SI Appendix*, Fig. S5 *D* and *E*). *HLA-E* mRNA, which encodes a factor reported to inhibit natural killer cell-mediated lysis (23–25), was expressed by giaSCs (*SI Appendix*, Fig. S5 *E* and *F*). In summary, transplanted giaSCs can survive long enough (20 d and 8 d respectively) to achieve significant therapeutic effects in repairing of skin wounds and small intestinal damage.

giaSCs are nontumorigenic in vivo. Two types of immunodeficient mice, nude and NOG, were used for tumorigenicity assays. 1M of giaSCs were transplanted subcutaneously into each mouse. Nude mice (n = 5) were observed for 4 mo, and NOG mice (n = 5) were observed for 6 mo. No teratomas or any neoplasms were observed at the endpoints (*SI Appendix*, Table S1). Furthermore, in vitro proliferation of giaSCs was limited to eight passages in the A/G system. *TERT*, which encodes the telomerase reverse transcriptase that restores or extends telomere length and thus confers cell immortality and is highly expressed in pluripotent stem cells and many tumors. However, *TERT* was not expressed by giaSCs (*SI Appendix*, Fig. S5*G*). These results demonstrated that, unlike human pluripotent stem cells (26), giaSCs have limited proliferation capability and are not tumorigenic, and thus are safe for stem cell therapy.

The in vitro differentiation potential of giaSCs. In addition to the main findings from the in vivo experiments, we have also tested the potential of giaSCs to differentiate into neural (ectoderm), osteogenic (mesoderm), and hepatic (endoderm) lineages in vitro. Incubation of giaSCs in commercial neural differentiation medium resulted in emergence of neurosphere-like colonies that stained positive for the neural specific markers Nestin and β3-tubulin (Fig. 1*N*). The differentiated cells derived from these colonies also expressed Nestin and β3-tubulin (*SI Appendix*, Fig. S6*A*). After 15 d in the neural differentiation medium, the cells exhibited typical neuron morphology (Fig. 1*O* and *SI Appendix*, Fig. S6*B*) and expressed neural stem cell marker MSI2 and mature neuron marker NeuN (Fig. 1*P*). Under the same conditions, neither m-GCs nor UC-MSCs, the parental cells of giaSCs, differentiated into cells with such neural morphologies. They did not express neural markers (*SI Appendix*, Fig. S6 *C* and *D*). When incubated in a commercial osteogenic differentiation medium, giaSCs differentiated into osteoblast-like cells that were positively stained with Alizarin Red, a marker for calcium-containing osteocytes (Fig. 1*Q*). In the A/G system that created hepatic environment, giaSCs expressed hepatic proteins albumin and AFP (Fig. 1*R*). These results showed that giaSCs may be able to differentiate into cells originating from the three germ layers.

Derivation and Characterization of giaSCs.

Derivation of guide cell precursors from human peripheral blood. Guide cell precursors were derived from adult human peripheral blood via high-speed centrifugation. The freshly isolated cells were 2 to 6 μm in diameter and they have nuclei as shown by Hoechst 33342 dye. The nucleus-to-cytoplasm ratio of these cells was very high as measured by fluorescence microscopy (Fig. 2*A*). More than 90% of freshly isolated cells showed undetectable intracellular esterase activity (Fig. 2*B*) and a very low level of transcriptomic activity (*SI Appendix*, Fig. S6*E*), indicating a dormant state. We refer to these cells as pre-GCs. The estimated frequency of pre-GCs was 800,000 to 1,500,000 cells per mL of blood as measured by flow cytometry based on blood samples from 100 adult donors. When not grown in our special medium, pre-GCs died within 2 to 5 d. We speculate that these cells were previously uncharacterized due to their small size, rarity compared to other blood cells and special survival conditions in vitro.

Activation and maturation of pre-GCs in vitro. To activate pre-GCs, we used medium conditioned by human hepatic HepaRG cells to establish an activation/growth (A/G) system. After overnight incubation in this A/G system, over 90% of pre-GCs had transcriptional activity with AO staining of DNAs and RNAs (*SI Appendix*, Fig. S6*F*) and translational activity as shown by Calcein Red-AM staining of intracellular esterase (Fig. 2*B* and *SI Appendix*, Fig. S6*G*). Upon continued culturing in the A/G system, these activated GCs increased in cellular size, showed adherent growth, and formed colonies (Fig. 2*C*). During 18 d of culturing, the morphology of the cells had changed dramatically from round to enlarged and flattened (Fig. 2*D*). A large number of granules aggregated in the central region of these cells, and the cytoplasm thus showed two distinct regions under light microscopy: a dark region containing granules and a transparent region with very few granules (Fig. 2*D*). Acridine orange (AO) staining revealed that abundant RNAs were packaged in the
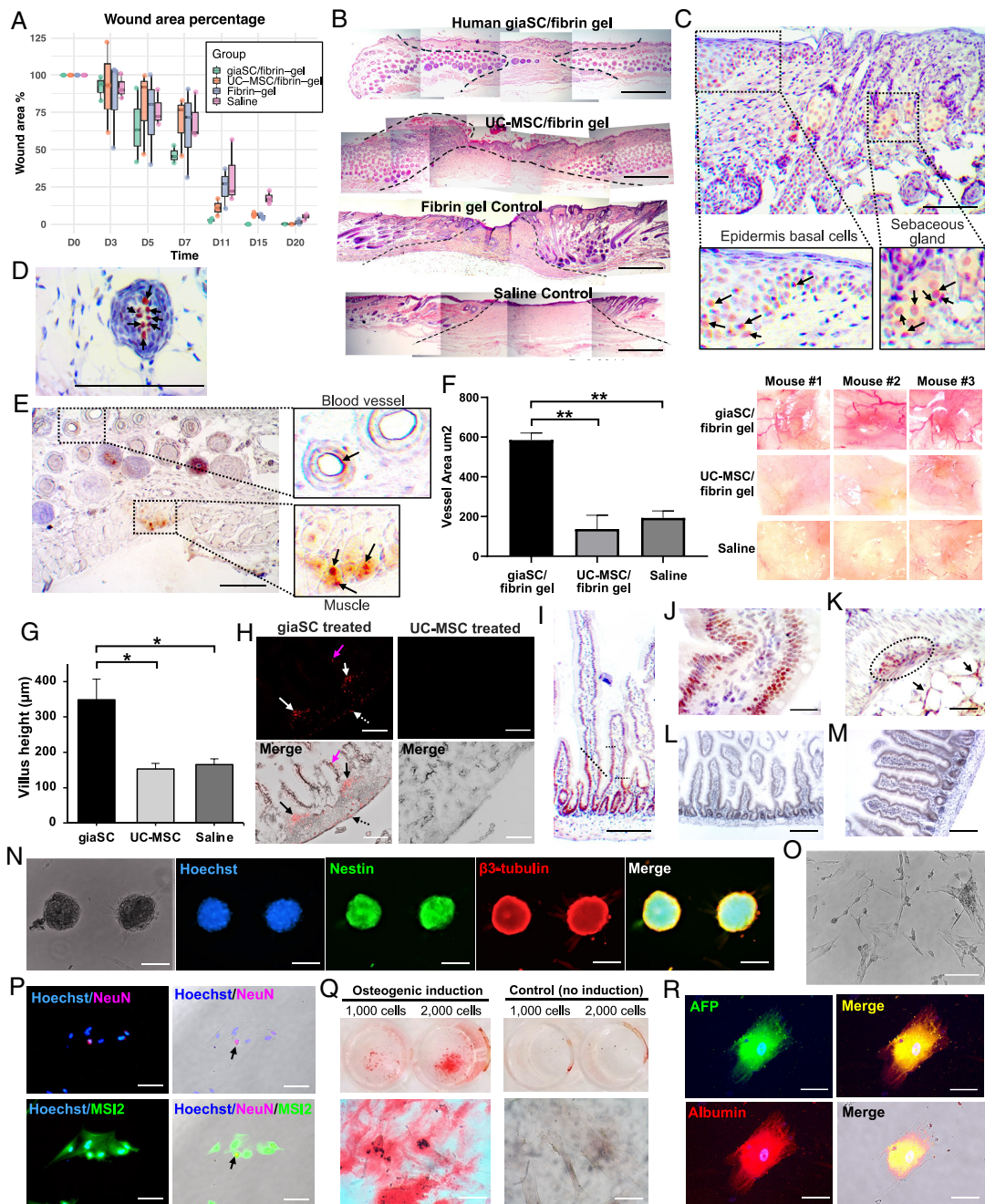
Fig. 1. giaSCs have high plasticity in vivo and in vitro. (*A–F*) Full-thickness excisional skin wounds were created by a biopsy punch in wild-type FVB mice. Wound sites were treated topically with human giaSC/fibrin gel or human UC-MSC/fibrin gel, fibrin gel only, or saline (n = 3 in each group). Skin wound sites were harvested on day 20 post treatment. (*A*) Wound area percentage (giaSC/fibrin gel compared to three control groups, *t* test *P < 0.05). (*B*) Representative H&E images of skin tissues from wound sites on day 20. (Scale bar, 1,000 μm.) (*C–E*) Representative images of tissue from wound site treated with giaSCs/fibrin gel stained with anti-human Ku80 antibody showing (*C*) epidermis basal cells and sebaceous glands, (*D*) hair follicles, and (*E*) blood vessels and muscles (arrows indicate human Ku80^{+} cells). (Scale bar, 200 μm.) (*F*) Blood vessel areas in wound regions (n = 3, *t* test **P < 0.01). (*G–M*) FVB mice were dosed via three intraperitoneal injections of LPS, and 3 d after the last LPS injection, mice were treated via retro-orbital injection with Qtracker 625-labeled human giaSCs (n = 10), Qtracker 625-labeled human UC-MSCs (n = 10), or saline (n = 8). As an additional control, mice untreated with LPS were treated via retro-orbital injection with human giaSCs (n = 3). Mice were killed on day 8 post treatment and intestinal tissue samples were harvested and analyzed. (*G*) Villus heights (n = 3, *t* test *P < 0.05). (*H*) Representative images of small intestinal tissue sections with fluorescence due to giaSCs indicated in the crypts (solid arrows), at the *Bottom* of the mucosal layer (dotted arrows), and along the villi (magenta arrows). No fluorescent signal was detected in sections treated with human UC-MSCs labeled with Qtracker 625. (Scale bar, 200 μm.) (*I–K*) Representative images of small intestinal tissue section from mouse treated with giaSCs stained with anti-human Ku80 antibody (red-brown) demonstrating positive staining: (*I*) at the crypts and bottom of the mucosal layer (mucosal layer below dotted lines), scale bar, 200 μm, (*J*) of simple columnar epithelial cells aligning along both sides of the villi, scale bar, 50 μm, and (*K*) in the smooth muscle layer (within dotted circle) and in the adipose tissue cells in the mesentery (black arrows). (Scale bar, 50 μm.) No positive staining was observed in the control groups (*L* and *M*): (*L*) Representative image of small intestinal tissue of mouse treated with human UC-MSCs stained with anti-human Ku80 antibody. (Scale bar, 200 μm.) (*M*) Representative image of small intestinal tissue of mouse not treated with LPS and transplanted with human giaSCs stained with anti-human Ku80 antibody. (Scale bar, 200 μm.) giaSCs were induced to differentiate into neural cells in vitro: (*N*) Images of cell colonies resulting from incubation of giaSCs for 7 d in neuronal differentiation medium; colonies were positively stained for Nestin and β3-tubulin. (Scale bar, 200 μm.) (*O*) Images of cells resulting from 15-d incubation of giaSCs in the neural differentiation medium, showing emergence of neural cell morphology. (Scale bar, 200 μm.) (*P*) Images of cells resulting from 15-d incubation of giaSCs in the neural differentiation medium, the cells were positively stained for MSI2 (neural stem cell marker) and NeuN (neuron marker) (arrow). (Scale bar, 100 μm.) (*Q*) Images of cells resulting from incubation of giaSCs in osteogenic differentiation medium, which was positively stained with Alizarin Red. (Scale bar, 200 μm.) (*R*) Images of cells resulting from incubation of giaSCs under conditions that mimic the hepatic environment stained for albumin and AFP, both markers were positive. (Scale bar, 100 μm.)
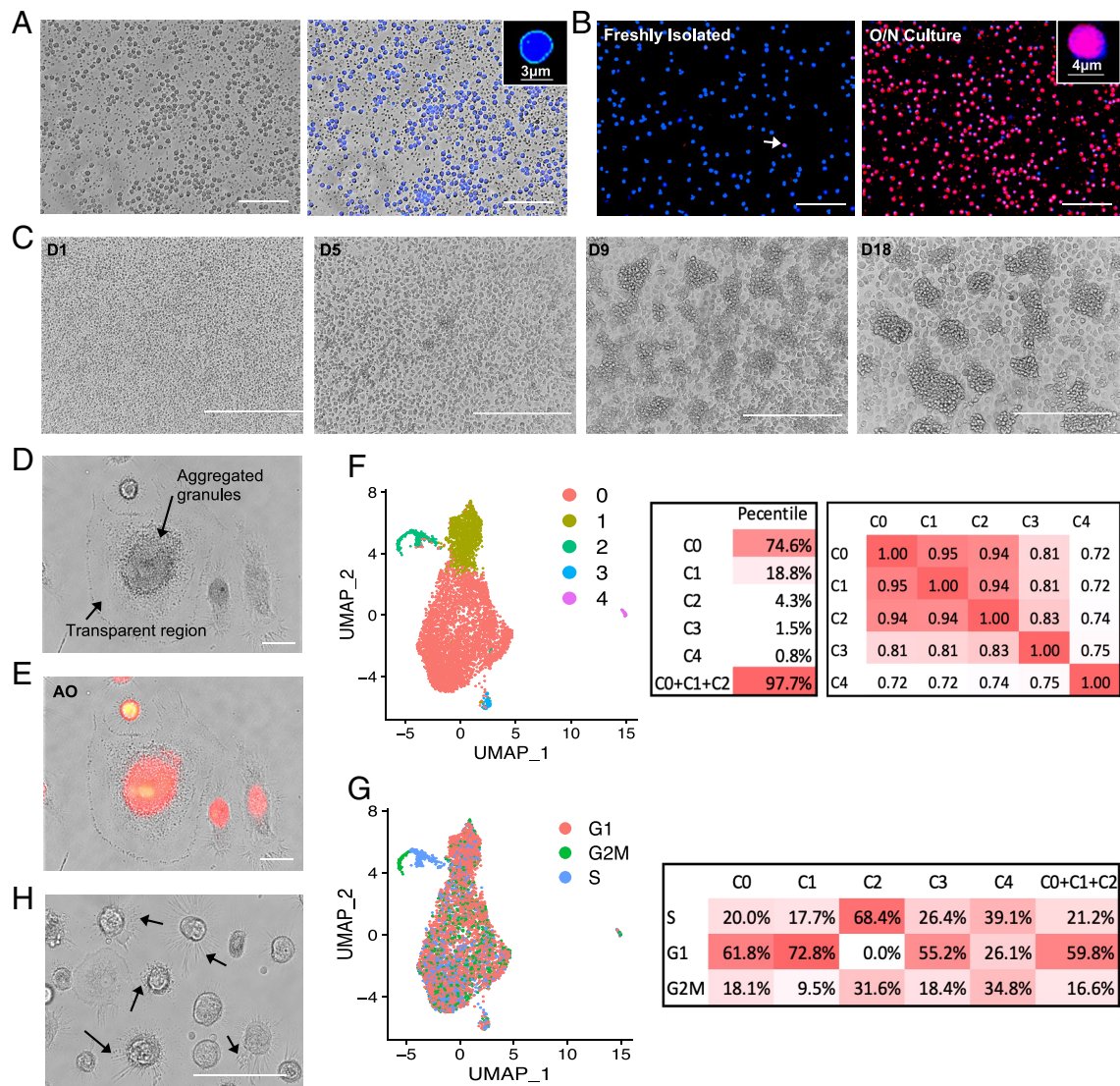
Fig. 2. Guide cells are dormant when isolated from human peripheral blood and can be activated and matured in vitro. (*A*) Phase-contrast micrograph (*Left*) and fluorescent images of freshly isolated, nucleated pre-GCs stained with Hoechst 33342 (blue). (Scale bar, 50 μm.) (*B*) Images of freshly isolated pre-GCs (*Left*) and GCs cultured overnight (*Right*) stained with Calcein Red-AM for esterase activity (cytoplasm; magenta, arrows) and with Hoechst 33342 (nuclei; blue). (Scale bar, 50 μm.) (*C*) Phase contrast images of GCs after 1, 5, 9, and 18 d (*D*) of culture in the A/G system. (Scale bar, 400 μm.) (*D*) Image of GCs after 18 d in culture. (Scale bar, 20 μm.) (*E*) Image of GCs after 18 d in culture stained with AO (merge; red for RNA; green for dsDNA). Aggregated granules containing RNAs in the central region are surrounded by a transparent region. (Scale bar, 20 μm.) (*F*) Correlation of clusters C0, C1, and C2 from scRNA-seq data of m-GCs in vitro culture on day 18. (*G*) Cell cycle analysis of m-GCs in vitro culture on day 18. (*H*) Phase contrast image of m-GCs on day 3 after passaging from the 18-d culture. Cells show aggregated granules in the cytoplasm and pseudopodia surrounding and projecting from the cell bodies (arrows). (Scale bar, 100 μm.)

granules (Fig. 2*E*). The cells containing RNAs-rich granules are referred to as m-GCs.

m-GCs were a relatively homogeneous population, as revealed by the clustering analysis of the single-cell RNA-seq (scRNA-seq) data. Five distinct clusters were identified. Clusters C0 (74.6%), C1 (18.8%), and C2 (4.2%) exhibited high Pearson correlation coefficients (>0.94) between mean expression profiles. Based on this high correlation, we classified them collectively as m-GCs, and these cells accounted for 97.7% of the entire cell population after 18 d of culture in the A/G system (Fig. 2*F*).

m-GCs lack self-renewal capability and can release granules.
m-GCs were weakly proliferative with 59.8% in G1 phase and 21.2% in S phase (Fig. 2*G*). Compared to newly generated giaSCs, m-GCs had lower levels of the proliferation marker *CCND1* and higher levels of *RB1*, which encodes a factor that halts the cell cycle at the G1/S checkpoint (*SI Appendix*, Fig. S5*H*). The morphology of m-GCs continued to change after passaging, and we observed many pseudopodia surrounding and projecting from the cell

bodies to release granules (Fig. 2*H*). During continued culture in the A/G system for 8 wk, m-GCs rarely proliferated, and cell deaths were observed (*SI Appendix*, Fig. S6*H*). This indicates that m-GCs lack self-renewal capability and thus are not stem cells. These data do, however, suggest that m-GCs may communicate with other cells by transported granules.

m-GCs communicate with UC-MSCs via tunneling nanotubes. To investigate whether granules secreted by m-GCs are taken up by other cells, UC-MSCs labeled with a green fluorescent dye (Calcein AM) were added into an adherent culture of m-GCs labeled with a red fluorescent dye (Qtracker 625) and incubated in the A/G System (Fig. 3 *A–C*). Between 12 and 24 h in coculture, m-GCs became nonadherent and started to communicate with the UC-MSCs, and the UC-MSCs formed colonies (Fig. 3*D*). Subsequently, many of the m-GCs surrounded and projected tunneling nanotubes (TNTs) into the colonies (Fig. 3*D* and *SI Appendix*, Fig. S6*I*). The red fluorescent granules from the m-GCs were transported through the TNTs into the UC-MSCs,
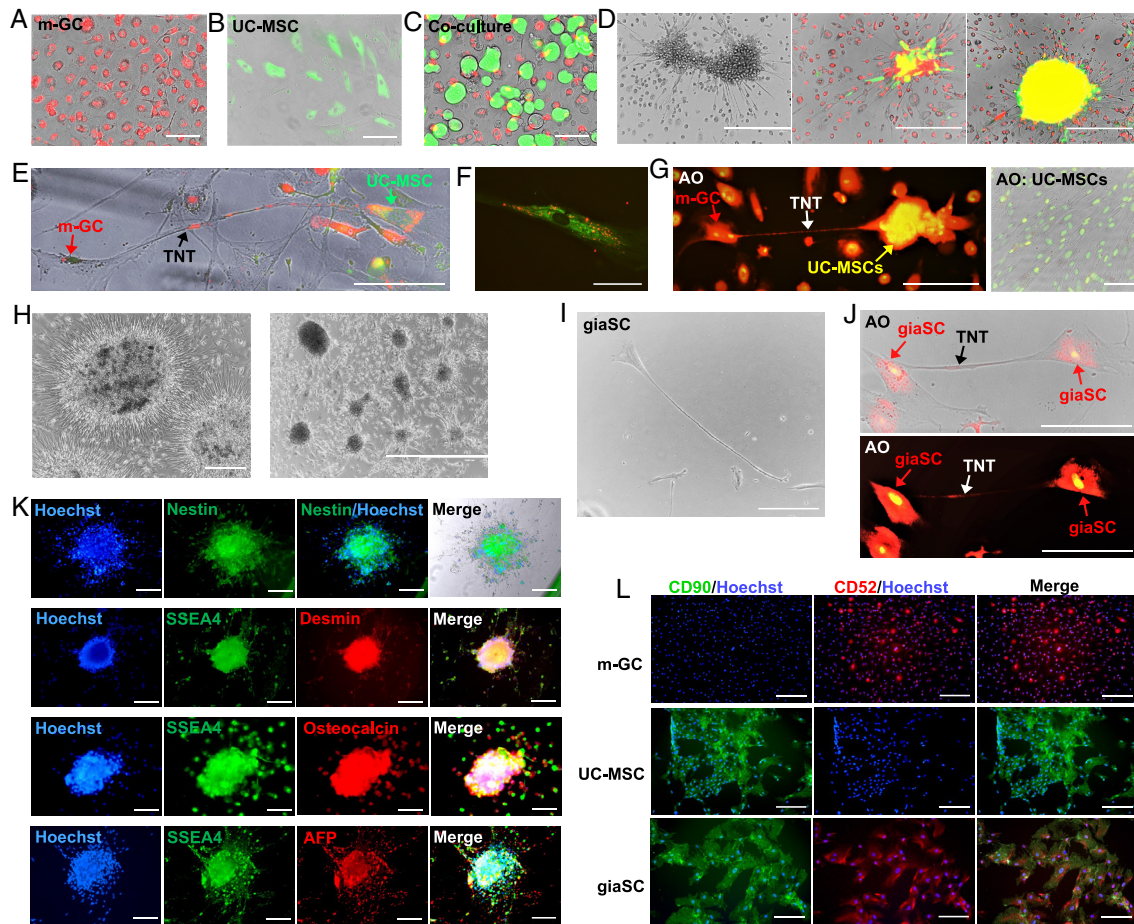
Fig. 3. m-GCs transfer RNA-loaded granules into UC-MSCs to generate giaSCs. (*A–C*) Images of (*A*) Qtracker 625-labeled human m-GCs (red) and (*B*) Calcein AM-labeled human UC-MSCs (green) were (*C*) cocultured in the A/G System. (Scale bar, 100 μm.) (*D*) Images after 12 h in coculture. Cellular contents of m-GCs (red) were transported into UC-MSCs (yellow). (Scale bar, 400 μm.) (*E*) Image after 12 h in coculture showing one-way transport of red granules from m-GCs to UC-MSCs (green) via TNTs. (Scale bar, 50 μm.) (*F*) Image after 12 h in coculture showing fluorescent green color cytoplasm of UC-MSCs containing red granules from m-GCs. (Scale bar, 20 μm.) (*G*) Image of TNT transportation between m-GC connected with UC-MSC shows that AO (Fluorescent red) RNA-rich granules from m-GC were transferred into green cytoplasm of UC-MSCs. (Scale bar, 100 μm.) (*H*) Phase contrast images in coculture show that the embryoid body–like colonies were formed on day three and cells migrated out of these colonies. [Scale bars, 200 μm (*Left*) and 1,000 μm (*Right*).] (*I*) Phase contrast image of giaSCs showing triangular body and filiform pseudopodium-like structure. (Scale bar, 100 μm.) (*J*) Images of giaSCs connected via TNTs in which AO-stained RNA-rich granules were transported from m-GC (red). (Scale bar, 50 μm.) (*K*) Images of giaSC colonies with Hoechst 33342 labeled nuclei, showing Nestin⁺ neural cell marker (ectoderm), Desmin+ myocyte marker (mesoderm), Osteocalcin⁺ osteoblast marker (mesoderm), AFP⁺ hepatocyte marker (endoderm), and SSEA4+. (Scale bar, 200 μm.) (*L*) Images of m-GCs, UC-MSCs, and giaSCs were stained with Hoechst 33342 and labeled with CD90 (green) and CD52 (red) antibodies. (Scale bar, 200 μm.)

which thus turned yellow (Fig. 3*D* and Movie S1). TNTs were also observed between single m-GC and single UC-MSC, and granules were transported through these tubes (Fig. 3*E*). Transportation was one way, from m-GCs to UC-MSCs, because no substances labeled with green fluorescence were detected in the TNTs and m-GCs remained red (Fig. 3 *E* and *F*). The granules from the m-GCs were transported in the form of clusters through the elastic TNTs (Fig. 3*E*). AO staining showed that the granules transported from m-GCs into UC-MSCs contained RNA (Fig. 3*G* and *SI Appendix,* Fig. S6*J*). At between 2 and 5 d in coculture, the colonies expanded in three dimensions and formed embryoid body–like structures, and cells proliferated and migrated radially out of the colonies (Fig. 3*H*). After dissociation of the colonies from the coculture, the residual m-GCs continued to release RNA-rich granules into the extracellular environment (*SI Appendix,* Fig. S6*K*). While m-GCs died after losing their RNA-rich granules (*SI Appendix,* Fig. S6*L*), the cells dissociated from the colonies continued to grow (*SI Appendix,* Fig. S6*L*).

giaSCs emerge from colonies formed by interaction of m-GCs with UC-MSCs. The emerged cells from the embryoid body–like colonies after m-GCs communicated with UC-MSCs were named

guide-integrated adult stem cells or giaSCs that were dissociated for analysis and in vivo transplantation. giaSCs show self-renewal capability for eight passages in the A/G system. The giaSCs have unique triangular-shaped bodies with filiform pseudopodia that differ from the morphologies of m-GCs and UC-MSCs (Fig. 3 *I* and *J*). We observed that giaSCs are able to connect to each other through TNTs (Fig. 3*J* and *SI Appendix,* Fig. S6*M*). The cytoplasm of giaSCs contained granules enriched in RNAs that could be transported via TNTs between giaSCs (Fig. 3*J*). giaSCs gained higher levels of transcription than UC-MSCs (Fig. 3 *G, Right*). The giaSC colonies express representative markers of each of the three germ layers: Nestin, Osteocalcin and Desmin, and AFP (Fig. 3*K*).

giaSCs express different surface markers compared to m-GCs and UC-MSCs as shown by IF, flow cytometry, and RNA-seq. giaSCs expressed both markers CD90 and CD52, whereas m-GCs expressed only CD52 and UC-MSCs only express CD90 (Fig. 3*L*). giaSCs also expressed CD49f, CD105, CD73, CD44, and CD56 (*SI Appendix,* Figs. S4 and S5*A*), did not express CD34, CD3, CD19, or CD20, and had low levels of expression of CD45 (Fig. 4*A* and *SI Appendix,* Figs. S4 and S5*A*). m-GCs were positive
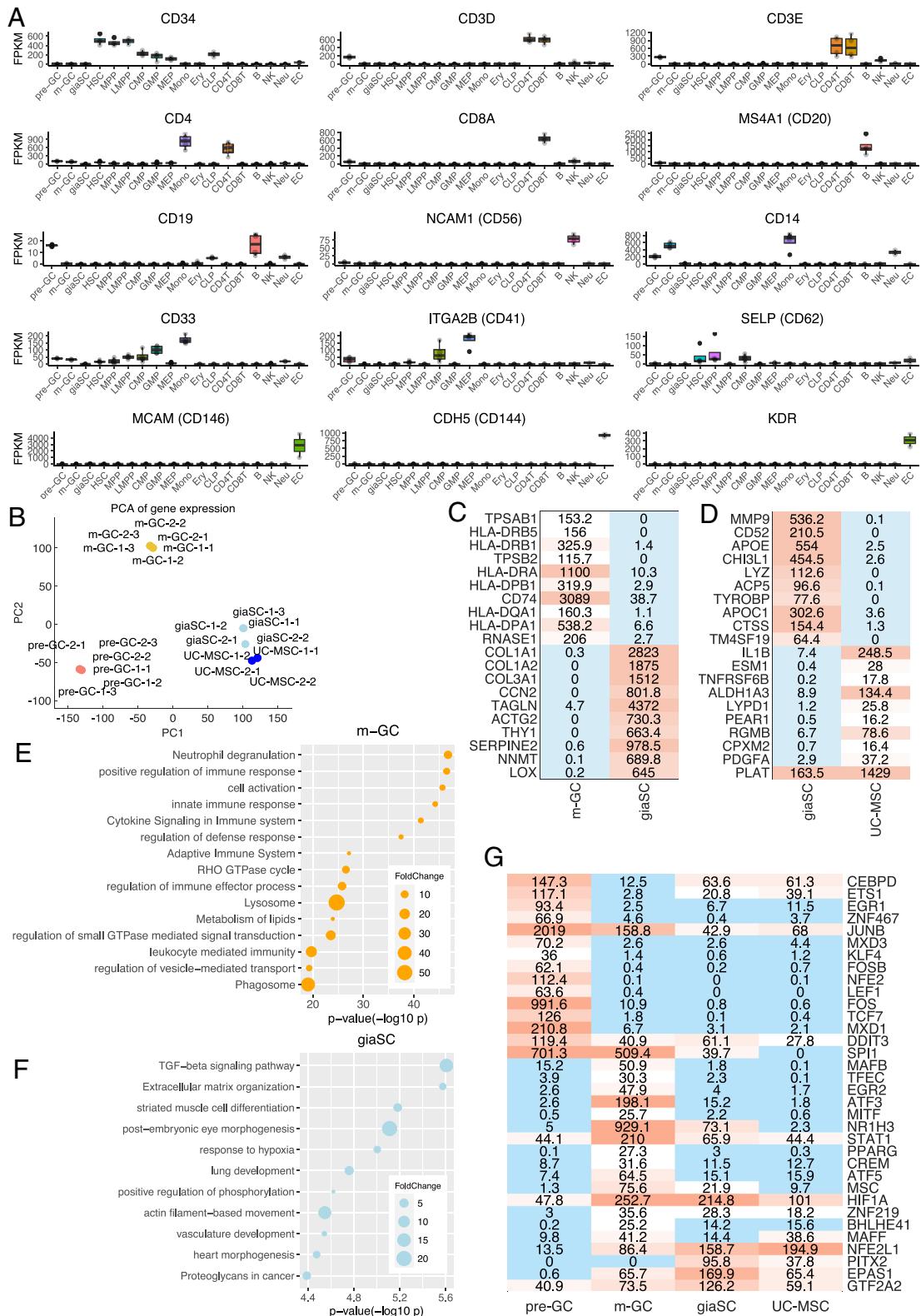
Fig. 4. giaSCs are transcriptomically distinct from pre-GCs, m-GCs, giaSCs, and other cells. (*A*) Expression of blood lineage marker genes and endothelial marker genes in bulk RNA-seq data for pre-GCs, m-GCs, giaSCs, HSCs, multipotent progenitors (MPP), lymphoid-primed multipotent progenitor (LMPP), common myeloid progenitors (CMP), granulocyte macrophage progenitors (GMP), megakaryocyte-erythroid progenitors (MEP), monocytes (Mono), erythroid cells (Ery), common lymphoid progenitors (CLP), CD4+ T cells (CD4T), CD8+ T cells (CD8T), B cells (B), natural killer cells (NK), neutrophils (Neu), and vein ECs. Boxplots represent minima, 25% quantile, median, 75% quantile, and maxima. Individual samples are plotted in gray points. (*B*) Principal component analysis of gene expression in pre-GCs, m-GCs, giaSCs, and UC-MSCs. (*C* and *D*) Top 20 differentially expressed genes between (*C*) m-GCs and giaSCs. (*D*) Top 20 differentially expressed genes between giaSCs and UC-MSCs. Colors indicate average FPKM across each cell type. (*E*) Functional enrichment of 1,901 genes that are prominently expressed in m-GCs but not in giaSCs and UC-MSCs. (*F*) Functional enrichment of 181 genes that exhibit higher expression in giaSCs compared to m-GCs and UC-MSCs. (*G*) Dynamic transcription factors identified by comparison of pre-GCs with m-GCs and of giaSCs and UC-MSCs. Colors indicate average FPKM across each cell type.

for CD49f, CD105, CD45, and CD44 (*SI Appendix*, Figs. S4 and S5*A*), did not express CD73, CD3, CD19, CD20, and CD56, and express low levels of CD34 (Fig. 4*A* and *SI Appendix*, Figs. S4 and S5*A*). Except for the very low expression level of *POU5F1* (which encodes Oct4), giaSCs and m-GCs did not express other key pluripotency markers, such as *Sox2*, *Nanog*, or *Lin28A* (*SI Appendix*, Fig. S5*G*).

giaSCs have distinct transcriptional profile compared to m-GCs and UC-MSCs. Principal component analysis (Fig. 4*B*) and clustering analysis (*SI Appendix*, Fig. S7*A*) of RNA-seq data showed that the cellular state of giaSCs was between those of m-GCs and UC-MSCs with closer proximity to UC-MSCs. This observation is consistent with our finding that giaSCs were generated from UC-MSCs under the guidance of m-GCs. With a fold change threshold of 2, a total of 4,511 genes exhibited differential expression between m-GCs and giaSCs (Fig. 4*C*), and 1,131 genes manifest differential expression between giaSCs and UC-MSCs (Fig. 4*D*). By applying a criterion where the mean fragments per kilobase of transcript per million mapped reads (FPKM) for UC-MSCs is less than 1 (indicating very low or background-level expression) and the fold change (FC) is greater than 2, where FC=(FPKM in giaSC)/(1 + FPKM in UC-MSC), we identified 194 genes expressed in giaSCs that were not transcribed in UC-MSCs. Using a more stringent cutoff of FPKM < 0.1 for UC-MSCs and FC > 5, we still identified 54 genes that were not transcribed in UC-MSCs but became activated in giaSCs (*SI Appendix*, Table S2). Further investigation uncovered 1,901 genes that were prominently expressed in m-GCs but not in giaSCs and UC-MSCs. These genes were associated with neutrophil degranulation (Fig. 4*E*), which suggested the possibility that m-GCs employed established degranulation mechanisms to deliver bioinformation materials to neighboring cells or into the extracellular space. Finally, there were 181 genes with higher expression in giaSCs than in m-GCs and UC-MSCs (FC > 2). Biological processes associated with these genes such as TGF-β signaling, extracellular matrix organization, and organ development (Fig. 4*F*) may be important for the plasticity of giaSCs.

Among the 1,131 genes differentially expressed (FC > 2) between giaSCs and UC-MSCs, 607 genes were expressed more highly in giaSCs than in UC-MSCs. Of these, 422 genes (69.5%) exhibited higher expression in m-GCs than in UC-MSCs. Further analysis showed that there was a significant overlap between the genes differentially expressed in giaSCs versus UC-MSCs and in m-GCs versus UC-MSCs (Fisher's exact test P = 4.06e-248, OR = 19.59, *SI Appendix*, Table S3). Additionally, 2,527 genes were expressed at significantly higher levels in UC-MSCs than in m-GCs, and 524 genes expressed at higher levels in UC-MSCs than in giaSCs. 361 genes overlapped with Fisher's exact test P = 1.41e-195 and OR = 16.57 (*SI Appendix*, Table S4). This robust pattern was consistent with the hypothesis that the differences between giaSCs and UC-MSCs were due to the influence of m-GC guidance on the UC-MSCs.

GCs and giaSCs are distinct from known reference cell types. We systematically compared the gene expression profiles of GCs and giaSCs with the 573 reference RNA-seq samples available in ENCODE (Dataset S1). We identified 518 genes expressed in pre-GCs, 360 genes in m-GCs, and 67 genes in giaSCs that exhibited significantly higher expression levels compared to all reference cell types (FC > 2, *SI Appendix*, Fig. S7*B*). The gene expression pattern in m-GCs was more highly correlated with gene expression patterns in blood cells (Spearman correlation ranging from 0.83 to 0.87, *SI Appendix*, Fig. S7*C*). We next evaluated correlations between expression patterns with four endothelial cell (EC) types (vein, umbilical vein, coronary artery, and pulmonary artery). The Spearman correlation between gene expression patterns of giaSCs and ECs was lower than that between giaSCs and mesenchymal stromal cells (MSCs), and the correlations between m-GC and EC expression patterns were also lower than those between blood cell and EC expression patterns (*SI Appendix*, Fig. S7*C*), demonstrating that m-GCs and giaSCs are distinct from ECs. For example, expression of endothelial marker genes (*MCAM*, *CDH5*, and *KDR*) clearly differentiate m-GCs and giaSCs from ECs (Fig. 4*A*). giaSC gene expression patterns were more highly correlated with MSC and fibroblast gene expression patterns than that of any other of the cell types in the 573 reference samples (ranging from 0.91 to 0.92, *SI Appendix*, Fig. S7*C*). However, many genes were differentially expressed between giaSCs and MSCs and between giaSCs and fibroblasts (2,411 and 1,848 genes, respectively; FC > 2 and t test P value < 0.01), indicating that giaSCs are distinct from all known cell types.

m-GCs are distinct from known blood cell types. We conduct a more comprehensive comparison between GCs and various blood lineage cells using a bulk RNA-seq dataset encompassing 14 distinct human primary blood cell types (27, 28). We also compared scRNA-seq data from m-GCs and blood cells (29). In analysis of bulk RNA-seq data, we identified 567 genes with higher expression in pre-GCs than blood cells and 1,214 genes with higher expression in m-GCs than blood cells (FC > 2, *SI Appendix*, Fig. S8*A*). *CD34*, which encodes a major positive marker of HSCs, was expressed at very low levels or was not detectable in m-GCs and was not expressed by giaSCs (Fig. 4*A*). Furthermore, *CD3D*, *CD3E*, *CD4*, and *CD8A*, which are markers of T cells, *CD19* and *CD20* (also known as *MS4A1*), which are markers of B cells, *CD56* (also known as *NCAM1*), a marker of natural killer cells, and *CD41* (also known as *ITGA2B*) and *CD62* (also known as *SELP*), which are markers of platelets, were expressed at low levels or were not detected in pre-GCs, m-GCs, and giaSCs (Fig. 4*A*). It is worth mentioning that the freshly isolated pre-GCs were a heterogeneous cell population and may be mixed with some T cells and B cells. However, our bulk RNA-seq data on m-GCs consistently aligned with scRNA-seq data from m-GCs rather than from lymphocytes. (*SI Appendix*, Fig. S8*B*). Although both gene expression patterns from pre-GCs and m-GCs were more highly correlated with gene expression in monocytes and dendritic cells than those of other blood cell types (*SI Appendix*, Fig. S8 *C and D*), analysis at the scRNA-seq level clearly demonstrated a distinct identity for m-GCs. Collectively, these findings confirmed that m-GCs are not a previously characterized type of blood cell.

Transcriptional changes occur during activation and maturation of guide cells. A profound transition was observed in the transcriptomic landscape when pre-GCs were compared to m-GCs (Fig. 4*B*). The correlation between gene expression patterns of pre-GCs and m-GCs was approximately 0.85 (*SI Appendix*, Fig. S7*A*). A large number, 2,830, of genes were expressed at higher levels (FC > 2) in pre-GCs than m-GCs, whereas 2,774 genes had higher expression (FC > 2) in m-GCs relative to pre-GCs. Notably, the top 500 genes most specific to pre-GCs were enriched in functions associated with immune responses and the regulation of hematopoiesis (*SI Appendix*, Fig. S7*D*). The 500 genes most specifically expressed in m-GCs were associated with biological processes like lysosomes, small molecule transport, extracellular matrix organization, and lipid metabolism (*SI Appendix*, Fig. S7*E*). This molecular shift likely underpinned the transition from a dormant pre-GC state characterized by limited intracellular activity to the activated state of m-GCs, characterized by cell growth and the presence of RNA-containing granules. Furthermore, genes encoding a number of transcription factors (TFs) were differentially expressed in pre-GCs and m-GCs (Fig. 4*G*).

Discussion

The plasticity of stem cells is essential for their capability to adapt to the host tissue environment and repair damaged tissue in therapeutic applications. Pluripotent stem cells are able to differentiate into all types of cells in the human body and thus are hypothetically able to maintain tissue homeostasis and to repair virtually all types of tissue damage (9, 10). To date, however, no pluripotent stem cells have been proven to exist in human adults. Thus, an alternative mechanism may exist in adults to maintain tissue homeostasis and repair damage at the systemic level. Intercellular communication is critical for coordinating multicellular behavior, function, and fate within tissues (30, 31), and we reasoned that interactions between certain types of somatic cells could lead to the generation of high-plasticity stem cells that may play an important role in the maintenance of tissue homeostasis and the repair of damaged tissues at the systemic level in adults. In this paper, we report the derivation of pre-GCs from human blood. Upon in vitro activation and maturation, the pre-GCs developed into m-GCs that communicated with and transferred RNA-containing granules into UC-MSCs through tunneling nanotubes. Upon receipt and integration of this bioinformation, UC-MSCs underwent substantial changes in gene expression profile (e.g., hundreds of silenced genes were activated) as well as in morphology and cell–cell interaction properties, resulting in the generation of a highly plastic type of stem cell that we call giaSCs (illustrated in *SI Appendix*, Fig. S9).

Upon transplantation into mice, giaSCs maintained their stemness. In mouse models, treatment topically or systemically with human giaSCs led to repair of damaged tissues, skin, and intestine, respectively. Expression of human Ku80 was detected in multiple cell types in the regenerated tissues in mice (on day 20 in the reconstituted skin tissue and on day 8 in the repaired small intestine tissue). This indicates multitypes of local tissue constituent cells derived from human giaSCs are present in the repaired tissues for a duration long enough for significant tissue structure reconstitution to be observed. Interestingly, when giaSCs were systemically transplanted into wild-type mice without tissue damage, no human Ku80$^+$ cells were detected in the small intestinal tissue on day 8, suggesting that, under normal physiological conditions, exogenous giaSCs do not intervene in the maintenance of small intestinal tissue homeostasis even though the intestinal epithelium has a high self-renewal rate. In control experiments with the human UC-MSCs, no tissue reconstitution was observed and no human Ku80$^+$ cells were detected. Furthermore, giaSCs express high levels of genes encoding angiogenic factors and immune modulators, which may contribute to tissue repair and regeneration. Our results suggest that there are two possible mechanisms, which may not be mutually exclusive, for giaSC and its derivatives to contribute to tissue repair: 1) they may directly participate in tissue regeneration, and 2) they may also secrete growth factors, such as VEGF, and other active substances to indirectly promote tissue repair or regeneration.

Unlike pluripotent stem cells, giaSCs have limited self-renewal propensity and lack *TERT* expression. Perhaps due to this limited proliferation capability, no tumors were observed after injection of giaSCs into immunodeficient mice. Besides, giaSCs express very low levels of *POU5F1* (which encodes Oct4), and do not express other pluripotency markers such as *SOX2*, *NANOG*, or *LIN28A*. Furthermore, human giaSCs appear to have low immunogenicity and express genes encoding immunomodulators, which may enable them as xenogeneic cells to reside in mouse host tissues. In our transplantation experiments using immunocompetent mice, we did not observe acute rejection that usually occurs in transplantation between different species. Rather, the transplanted giaSCs survived a long enough period for multidirectional differentiation in the damaged tissue to achieve significant therapeutic effects in the repair of skin and small intestine tissues. Furthermore, the skin wounds in both immunodeficient mice (nude) and immunocompetent mice (wild type FVB) treated with human giaSCs showed similar repair effects on day 20. The presence of human Ku80$^+$ cells was detected at the repaired tissue sites in both groups, and a similar distribution pattern of human Ku80$^+$ cells was observed in the repaired skin tissue of both. These findings indicate that the skin constituent cells differentiated from giaSCs at least survived the acute immune rejection (which occurs within 1 to 2 wk) in the immunocompetent mouse hosts. Future studies will settle the question of whether giaSCs can achieve longer period of persistence after transplantation into immunocompetent mouse models, and explore the mechanism by which the transplanted giaSCs and giaSC-derived cells escape acute immune rejection in immunocompetent hosts.

The giaSCs were generated via cell–cell communication between guide cells and recipient cells. UC-MSCs were used as the recipient cell type in the experiments reported in this paper, but other types of somatic cells may also serve as recipient cells yielding high-plasticity stem cells or tissue-specific stem cells. For example, in preliminary experiments that will be reported in due course, we observed that communication between m-GCs and small intestinal epithelial cells led to stem cells that possess features and functions similar to those of the giaSCs described in this paper.

Future work will focus on isolating and analyzing the bioinformatic substances packaged in the granules present in m-GCs to investigate what types of bioinformatic substances are transferred into recipient cells. Given the intense AO staining of the granules and the transcriptomic changes in the UC-MSCs, we hypothesize that UC-MSCs received regulatory RNAs from the m-GCs. Several studies have shown that regulatory RNAs transmitted by extracellular vesicles are able to modulate chromatin structure and regulate gene expression (32–34). It is thus reasonable to speculate that RNAs from m-GCs are involved in the transcriptomic changes and possibly chromatin structural changes in the UC-MSCs.

In summary, we have shown that guide cells can be derived from human blood, activated, matured, and used to guide the generation of highly plastic giaSCs that, upon transplantation, can promote reconstitution of skin and intestinal tissue in mouse models. It will be of interest to study the origins of the guide cells and their functions during circulation in the peripheral blood, especially whether and how they can be activated in vivo to facilitate tissue homeostasis and repair by interaction with tissue-resident recipient cells. Because of their stemness properties, low immunogenicity, and nontumorigenicity, giaSCs have promise for use in regenerative medicine.

Materials and Methods

Human peripheral blood samples were collected by Stanford Blood Center with IRB approval (IRB 7 registration number 5136; protocol number 13942) and informed consent was obtained from all donors for research use. Human pre-GCs were isolated from the blood samples by high-speed centrifugation to obtain a cell pellet, which was then activated in an in-house A/G system and grew into m-GCs. m-GCs were cocultured with human UC-MSCs in the A/G system to form cell colonies, from which giaSCs were collected and further analyzed via flow cytometry, IF staining, in vitro induction assays, RNA sequencing and analysis, and in vivo transplantation models in mice. giaSCs' in vivo plasticity was examined in skin tissue reconstitution assay as well as LPS-induced small intestinal tissue damage model, and the data were analyzed using histology, IHC staining, in situ hybridization assay, et al. Detailed information is provided in *SI Appendix*.

Author affiliations: [a]APstem Therapeutics, Inc., Fremont, CA 94538; [b]Department of Statistics, Stanford University, Stanford, CA 94305; [c]Department of Biomedical Data Science, Stanford University, Stanford, CA 94305; and [d]Bio-X Program, Stanford University, Stanford, CA 94305

1. B. Biteau, C. E. Hochmuth, H. Jasper, Maintaining tissue homeostasis: Dynamic control of somatic stem cell activity. *Cell Stem Cell* **9**, 402–411 (2011).
2. I. Banjac, M. Maimets, K. B. Jensen, Maintenance of high-turnover tissues during and beyond homeostasis. *Cell Stem Cell* **30**, 348–361 (2023).
3. A. D'Souza *et al.*, Current use of and trends in hematopoietic cell transplantation in the United States. *Biol. Blood Marrow Trans.* **26**, e177–e182 (2020).
4. E. Atilla, P. Ataca Atilla, T. Demirer, A review of myeloablative vs reduced intensity/non-myeloablative regimens in allogeneic hematopoietic stem cell transplantations. *Balkan Med. J.* **34**, 1–9 (2017).
5. M. S. Hu *et al.*, Embryonic skin development and repair. *Organogenesis* **14**, 46–63 (2018).
6. I. Usansky *et al.*, A developmental basis for the anatomical diversity of dermis in homeostasis and wound repair. *J. Pathol.* **253**, 315–325 (2021).
7. P. Du, J. Wu, Hallmarks of totipotent and pluripotent stem cell states. *Cell Stem Cell* **31**, 312–333 (2024).
8. K. Takahashi, S. Yamanaka, Induction of pluripotent stem cells from mouse embryonic and adult fibroblast cultures by defined factors. *Cell* **126**, 663–676 (2006).
9. National Research Council (US) and Institute of Medicine (US) Committee on the Biological and Biomedical Applications of Stem Cell Research, *Stem Cells and the Future of Regenerative Medicine* (National Academies Press, 2002), p. 112.
10. S. Yamanaka, Induced pluripotent stem cells: Past, present, and future. *Cell Stem Cell* **10**, 678–684 (2012).
11. B. Blum, O. Bar-Nur, T. Golan-Lev, N. Benvenisty, The anti-apoptotic gene survivin contributes to teratoma formation by human embryonic stem cells. *Nat. Biotechnol.* **27**, 281–287 (2009).
12. A. S. Lee, C. Tang, M. S. Rao, I. L. Weissman, J. C. Wu, Tumorigenicity as a clinical hurdle for pluripotent stem cell therapies. *Nat. Med.* **19**, 998–1004 (2013).
13. I. B. B. Silva, C. H. Kimura, V. P. Colantoni, M. C. Sogayar, Stem cells differentiation into insulin-producing cells (IPCs): Recent advances and current challenges. *Stem Cell Res. Ther.* **13**, 309 (2022).
14. S. Yamanaka, Pluripotent stem cell-based cell therapy-promise and challenges. *Cell Stem Cell* **27**, 523–531 (2020).
15. A. Oikonomopoulos, T. Kitani, J. C. Wu, Pluripotent stem cell-derived cardiomyocytes as a platform for cell therapy applications: Progress and hurdles for clinical translation. *Mol. Ther.* **26**, 1624–1634 (2018).
16. T. Studemann *et al.*, Impulse initiation in engrafted pluripotent stem cell-derived cardiomyocytes can stimulate the recipient heart. *Stem Cell Rep.* **19**, 1053–1060 (2024).
17. A. Rustom, R. Saffrich, I. Markovic, P. Walther, H. H. Gerdes, Nanotubular highways for intercellular organelle transport. *Science* **303**, 1007–1010 (2004).
18. S. Li, M. Hu, H. P. Lorenz, Treatment of full-thickness skin wounds with blood-derived CD34(+) precursor cells enhances healing with hair follicle regeneration. *Adv. Wound Care (New Rochelle)* **9**, 264–276 (2020).
19. A. Mol *et al.*, Fibrin as a cell carrier in cardiovascular tissue engineering applications. *Biomaterials* **26**, 3113–3121 (2005).
20. Y. Li, H. Meng, Y. Liu, B. P. Lee, Fibrin gel as an injectable biodegradable scaffold and cell carrier for tissue engineering. *Sci. World J.* **2015**, 685690 (2015).
21. J. Allard *et al.*, Immunohistochemical toolkit for tracking and quantifying xenotransplanted human stem cells. *Regen. Med.* **9**, 437–452 (2014).
22. H. M. Li *et al.*, Berberine protects against lipopolysaccharide-induced intestinal injury in mice via alpha 2 adrenoceptor-independent mechanisms. *Acta Pharmacol. Sin.* **32**, 1364–1372 (2011).
23. V. M. Braud *et al.*, HLA-E binds to natural killer cell receptors CD94/NKG2A, B and C. *Nature* **391**, 795–799 (1998).
24. S. L. Wooden, S. R. Kalb, R. J. Cotter, M. J. Soloski, Cutting edge: HLA-E binds a peptide derived from the ATP-binding cassette transporter multidrug resistance-associated protein 7 and inhibits NK cell-mediated lysis. *J. Immunol.* **175**, 1383–1387 (2005).
25. N. Lee *et al.*, HLA-E is a major ligand for the natural killer inhibitory receptor CD94/NKG2A. *Proc. Natl. Acad. Sci. U.S.A.* **9**, 5199–5204 (1998).
26. E. Lezmi, N. Benvenisty, The tumorigenic potential of human pluripotent stem cells. *Stem Cells Transl. Med.* **11**, 791–796 (2022).
27. M. Corces *et al.*, Lineage-specific and single-cell chromatin accessibility charts human hematopoiesis and leukemia evolution. *Nat. Genet.* **48**, 1193–1203 (2016).
28. L. Zhu *et al.*, Chromatin landscapes and genetic risk for juvenile idiopathic arthritis. *Arthritis Res. Ther.* **19**, 57 (2017).
29. X. Xie *et al.*, Single-cell transcriptomic landscape of human blood cells. *Natl. Sci. Rev.* **8**, nwaa180 (2021).
30. N. Polyakova, M. Kalashnikova, A. Belyavsky, Non-classical intercellular communications: Basic mechanisms and roles in biology and medicine. *Int. J. Mol. Sci.* **24**, 6455 (2023).
31. E. Armingol, A. Officer, O. Harismendy, N. E. Lewis, Deciphering cell-cell interactions and communication from gene expression. *Nat. Rev. Genet.* **22**, 71–88 (2021).
32. K. O'Brien, K. Breyne, S. Ughetto, L. C. Laurent, X. O. Breakefield, RNA delivery by extracellular vesicles in mammalian cells and its applications. *Nat. Rev. Mol. Cell Biol.* **21**, 585–606 (2020).
33. L. Statello, C. J. Guo, L. L. Chen, M. Huarte, Gene regulation by long non-coding RNAs and its biological functions. *Nat. Rev. Mol. Cell Biol.* **22**, 96–118 (2021).
34. S. Yang, S. H. Kim, E. Yang, M. Kang, J. Y. Joo, Molecular insights into regulatory RNAs in the cellular machinery. *Exp. Mol. Med.* **56**, 1235–1249 (2024).
35. S. Li *et al.*, Data from "Human stem cells with in vivo high plasticity generated by cell-cell communication." Gene Expression Omnibus. https://www.ncbi.nlm.nih.gov/geo/query/acc.cgi?acc=GSE242346. Deposited 5 September 2023.